Research Paper

Variability in luminescent lamination and initial ^{230}Th/^{232}Th activity ratios in a late Holocene stalagmite from northern Norway

Henriette Linge [a,b,]*, Andy Baker [c], Carin Andersson [b], Stein-Erik Lauritzen [a]

[a] Department of Earth Science, University of Bergen, Allégaten 41, NO-5007 Bergen, Norway
[b] Bjerknes Centre for Climate Research, Allégaten 55, NO-5007 Bergen, Norway
[c] School of Geography, Earth and Environmental Sciences, University of Birmingham, Edgbaston, Birmingham B15 2TT, UK

ARTICLE INFO

ABSTRACT

Luminescent lamination in a stalagmite from northern Norway is used to construct a ~2780-year long, floating record of annual growth rate. Thermal ionisation mass-spectrometric (TIMS) U–Th ages ($n = 12$) were determined along the growth axis and three subsample locations and ages (corrected and uncorrected for initial ^{230}Th/^{232}Th activity) were selected as anchor points for the floating chronology. On the basis of these anchor points, termination of growth occurred between AD 1729 and AD 1826. The annual banding records are used to evaluate the initial ^{230}Th/^{232}Th activity ratio adopted for correction of the U–Th ages. To achieve a reasonable fit between U–Th ages and estimates predicted by the anchored annual band age models, mean initial ^{230}Th/^{232}Th activity ratios of between 0.44 and 1.47 must be invoked. However, there remains a reasonable degree of scatter about the expected linear relationship between annual bands and U–Th chronology for individual subsamples indicating that the use of a single correction factor for Holocene stalagmites should be applied with caution.

Stalagmite growth rate fluctuates on annual to centennial scale. The growth termination of the stalagmite presented here could have been a result of environmental change associated with the Little Ice Age, or, possibly local percolation pathway changes after an $M_s \sim 6$ earthquake in the region in AD 1819. Stable-isotope data from the same axis of growth show a pattern similar to the large-scale growth rate variations, and these combined proxy records are interpreted as showing gradual cooling and/or shortening of the vegetation growth season for the last 3000 years.

© 2009 Elsevier Ltd. All rights reserved.

1. Introduction

Speleothems, such as calcium carbonate ($CaCO_3$) stalagmites, are important continental archives because they can record environmental changes. Precipitation of $CaCO_3$ occurs if CO_2 in seepage water with higher pCO_2 derived from the soil atmosphere degasses when entering caves with lower pCO_2. Stalagmite growth rate is a function of temperature, drip rate and Ca^{2+} concentration of the dripwater, and is therefore in principle linked to regional climate through the cave temperature, meteoric precipitation and soil activity (e.g. Baker et al., 1998; Dreybrodt, 1999; Kaufmann and Dreybrodt, 2004). Organic acids derived from the overlying soil zone can be trapped within the calcite, resulting in luminescent lamination (Baker et al., 1993; Shopov et al., 1994; McGarry and Baker, 2000; van Beynen et al., 2001).

Carbonate precipitates from caves can contain various proxy archives of palaeoclimatic and palaeoenvironmental change (e.g. Gascoyne, 1992; Lauritzen, 2003; Fairchild et al., 2006) that can be precisely and accurately dated by U–Th techniques (e.g. Ivanovich and Harmon, 1992; Bourdon et al., 2003; Richards and Dorale, 2003; van Calsteren and Thomas, 2006). The stable oxygen and carbon isotope composition of the stalagmite calcium carbonate ($\delta^{18}O_c$, $\delta^{13}C_c$) provides potential archives of climatological and hydrological conditions (e.g. Gascoyne, 1992; McDermott, 2004; Fairchild et al., 2006), such as the isotopic composition of rainwater, soil productivity, and cave temperature and ventilation.

Annual increments in stalagmites (e.g. Broecker et al., 1960; Genty and Quinif, 1996; Tan et al., 2006), typically occur as organic lamination, variations in calcite texture or fabric, or calcite–aragonite alternation, which allow precise determination of growth rates. Annual variation in calcite accretion and/or laminae frequency can thus record changing environmental conditions: e.g. double laminae have been shown to occur in years with high monthly or daily mean precipitation (Baker et al., 1999) or to represent both an autumn signal and a second spring meltwater-generated influx

of organic matter after extremely cold winters (Baker et al., 2002). Records with confirmed climate-respondent calcite accretion can potentially provide proxy data of annual and subannual resolution from terrestrial environments back to at least 500 ka, which is the practical limit for age determination using U–Th (e.g. Edwards et al., 1987), and would be highly useful in palaeoclimate research and for evaluating future climate change.

While there is a potentially wide range of useful information that can be derived from stalagmites, isolating a single climatic parameter is not straightforward in any of the proxies offered by stalagmite calcite, as temperature affects the isotopic composition both at the source and storage (e.g. ocean, soil) and during calcite precipitation in the cave. Moreover, individual compounds may respond differently to transport and storage. Finally, local environmental conditions (e.g. cave humidity, drip rate, water chemistry, and percolation pathway) affect the degree of equilibrium between calcite and dripwater, and may cause non-equilibrium fractionation due to kinetic isotope effects (e.g. Mickler et al., 2006).

Proxy data of annual/subannual resolution are expected to significantly improve our understanding of stalagmites as palaeoclimate repositories, allowing stalagmite records for example stable isotopes and trace metals to be compared to independent climate data and/or climate proxies such as tree-rings, corals, ice-cores and documentary data (see Jones et al., 2009 for a thorough review on the current status of high-resolution palaeoclimatology). This, however, would require firm chronological control of the stalagmite data in order to minimise ambiguities and uncertainties in stalagmite proxy response. In this study, we present a nearly 2800-year long late Holocene stalagmite record of luminescent lamination and use this to investigate initial $^{230}Th/^{232}Th$ activity ratios in detail. Our main emphasis has been to create a plausible age model for a floating annual growth record, but we also suggest a simplified palaeoclimate interpretation from the relationship between luminescence characteristics, annual growth rate variations and longer-term changes in stable-isotope composition.

2. High-latitude stalagmites and Scandinavian climate

Atmospheric circulation over Scandinavia is generally characterised by migratory cyclones within the North Atlantic zone of westerlies (Johannessen, 1970), or the North Atlantic Oscillation, being most intense during wintertime. A combination of the circulation patterns and orographic influence of the Scandinavian mountain chain results in coastal areas with meteoric precipitation maxima during winter and increasingly continental conditions increase eastward.

Stalagmite deposition in Norwegian caves is only possible in the absence of ice sheets and permafrost (Lauritzen, 1991a; Lauritzen, 1995), and preservation of pre-Holocene stalagmite deposits is rare due to sub-glacial flooding (filling and/or flushing) of the passages. Stalagmites from northwest Scandinavia display increased $\delta^{18}O_c$ values during the Little Ice Age (LIA) followed by lower $\delta^{18}O_c$ values during the last century (Linge, 1999; Linge et al., 2001b; Sundqvist, 2007). The negative correlation of $\delta^{18}O_c$ values with temperature is consistent with the temperature-dependent fractionation constant between calcite and water (O'Neil et al., 1969), but opposes the positive correlation between temperature and $\delta^{18}O$ values of meteoric precipitation. Despite the largest amount of meteoric precipitation usually being received during winter in coastal northern Norway, the duration and/or depth of frozen ground conditions during winter may cause the stable-isotope composition of high-latitude/altitude stalagmites to be biased towards the summer meteoric precipitation.

Typical $\delta^{13}C_c$ values in Norwegian stalagmites are often notably higher than those from mid latitude stalagmites, and while they are likely to depend on moisture and temperature conditions in the soil zone above (Linge et al., 2001b), the mechanism of $\delta^{13}C_c$ variation in high-latitude stalagmites remains poorly understood.

3. Cave setting and material

The L-03 stalagmite was collected from Larshullet, a cave situated in Rauvassdalen in the Rana region, approximately 15 km south of the Arctic Circle in northern Norway (Fig. 1a). The nearest outlet glacier of the Svartisen ice cap is today approximately 10 km from the cave. The Larshullet cave (Fig. 1b) is developed in stripe karst consisting of carbonates metamorphosed during the Caledonian orogeny (Lauritzen, 1991b). The entrance is at about 400 m above sea level (asl), and the cave passages are oriented subparallel to the western side of the Rauvassdalen valley. A few hundred metres away is the Lapphullet cave, where periodic speleothem deposition has occurred at least since 0.5 Ma ago (Lauritzen et al., 1990).

Local meteorological data is limited but show an annual mean temperature of +1.4 °C (AD 1982–1987), and a mean annual meteoric precipitation close to 1600 mm (AD 1982–2004) (station 79670, Rødvassdalen, 56 m asl, http://eklima.met.no). April through October have monthly mean temperatures above 0 °C, whereas April through August normally receive less than 120 mm precipitation. Snow cover is persistent from October to May (station 79640, Grønligrotta, 87 m asl, http://eklima.met.no). In the region, the vegetation growth season at low elevations spans from early May to late October (Aune, 1993), but is shorter at the elevation of the cave site. Monitoring of cave microclimate and stable isotopes in Søylegrotta, ca. 25 km to the east, has shown near-constant temperature and near-uniform stable-isotope composition for the cave compared to the meteoric precipitation at the surface (Lauritzen and Lundberg, 1999).

The Rana region has had a relatively high, constant seismic activity in the 20th century (e.g. Hicks et al., 2000), and experienced the largest known earthquake in Fennoscandia in recent times, an M_s 5.5–6.2 earthquake, in AD 1819. This is assumed to be the cause of lateral shifts in vertical growth axis occasionally observed in stalagmites in the area. Earthquakes can be a regionally important non-climatic factor for disturbance of stalagmite growth, not only by displacements of stalagmites themselves, but also indirectly by alterations inflicted on percolation pathways draining to the cave.

The L-03 stalagmite grew on a large block approximately 60 m from the cave entrance, with a mica schist roof thickness of about 50–60 m. The surface is dominated by alpine vegetation. The stalagmite measures 144 mm along the vertical growth axis, is beige in colour, translucent to opaque, and characterised by visible banding from top to the base. Zones of less massive calcite with non-coalescing crystals and substantial amounts of fine-grained detritus (Fig. 1c and d) characterise the apex area of the stalagmite. Luminescent laminae are found throughout the sample, suggesting that its dripwater experienced little mixing before reaching the cave chamber, and it is expected that proxy records from this sample should mirror the surface and/or cave environment in great detail. One distinct hiatus is found at about 110.5 mm from the top and marks a transition from overall opaque calcite with alternating coloured and white bands below, to overall translucent and coloured calcite above. It is unknown whether the hiatus represents a simple halt in precipitation or if it was formed by a corrosional event. Laminae were not counted below the hiatus, however, after confirming an annual nature of the banding this could in future be performed to reveal details on the hiatus.
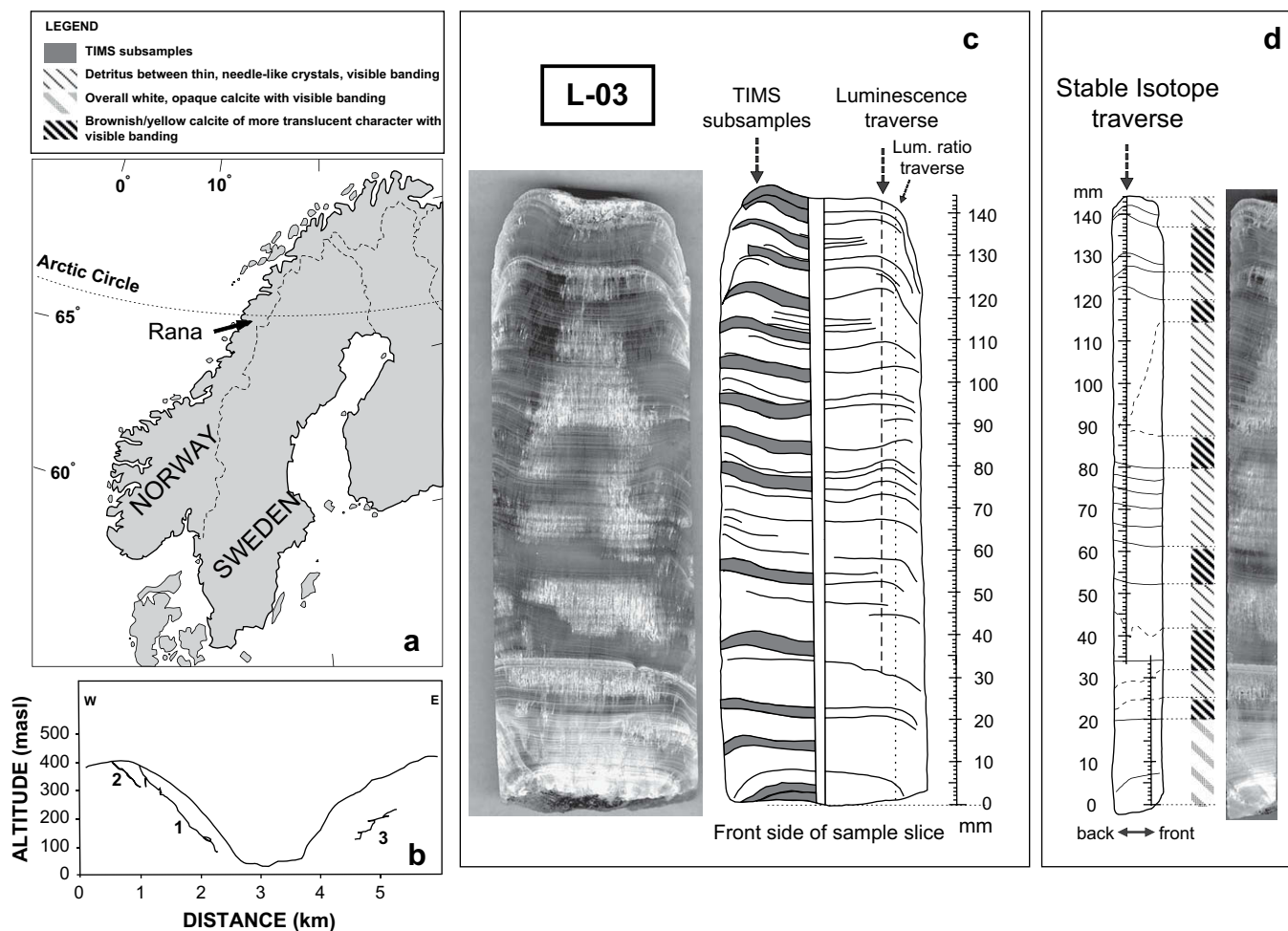
Fig. 1. a) Map of Scandinavia, arrow indicates position of Rana. b) Cross-section of Rauvassdalen. 1 = Larsgrotta, 2 = Lapphullet, 3 = Grønligrotta (from Lauritzen et al., 1990). c) Front side of L-03 sample slice, 144 mm from base to top. The left part of the sample has been used for TIMS U–Th dating (grey zones). The right part of the slice was used for stable isotopes (see Fig. 1d) and luminescent laminae analyses (vertical broken line). Thin, sub-horizontal lines indicate the most visible growth lines. d) Side view of the right part of the sample slice: stable isotopes have been measured along the vertical growth axis (mm scale, identical to the TIMS subsample reference scale). The shift in the position of the vertical growth axis was to avoid dust rich zones in the calcite. The legend to the simplified stratigraphy (positioned between the stable-isotope traverse and the corresponding image) is shown in the box above the map (a).

4. Analytical methods

The L-03 stalagmite was cut parallel to the growth axis and one slab (Fig. 1c) was cut in two along its growth axis. One part was dedicated for TIMS U–Th dating (Fig. 1c). The other part was polished and luminescent laminae were recorded along one traverse (Fig. 1c), and powder for stable-isotope analysis was sampled along another traverse (Fig. 1d).

Sample preparation and TIMS U–Th analysis were done at the Department of Earth Science, University of Bergen, following the description by Lauritzen and Lundberg (1999). Subsamples of 2–3 mm vertical thickness (Fig. 1c) and 300–1600 mg, were heated to 500 and 900 °C, dissolved in 7 N HNO_3 and gently heated for 5 h to equilibrate after addition of a triple (^{233}U–^{236}U–^{229}Th) tracer. Chemical separation and purification of U and Th included scavenging with Fe-precipitation, two sets of anion-exchange columns and final drydown with H_3PO_4. U and Th were loaded in filaments with silica gel and graphite, respectively, and U and Th-isotopic determinations were acquired on a ThermoFinnigan MAT 262 mass spectrometer using the SEM in peak-jumping mode (e.g. Lauritzen and Lundberg, 1999; Goldstein and Stirling, 2003). All U–Th ages are reported as years before AD 2000 with 2σ uncertainties.

The luminescence ratio (EX390/EX350 nm) was initially measured along the vertical axis of the sample (i.e. stable-isotope traverse), producing a ∼138 mm record as bottom and top were truncated to avoid edge effects producing misleading wavelength data. The ratio provides an indication of the degree of decomposition of the organic matter in the dripwater; fulvic acids are of lower molecular weight, are more readily soluble in water, and have more intense luminescence and shorter excitation and emission wavelengths than humic acids (Senesi et al., 1991; McGarry and Baker, 2000). A high ratio can therefore be taken to reflect a lesser degree of decomposition and as indicative of cool and/or wet conditions (Proctor et al., 2000).

For the analysis of luminescent laminae, standard UV microscopy techniques were used including a 320–420 nm excitation filter and a 420 nm barrier filter to view the emitted light (Baker et al., 1993). Overlapping images along a 110.6 mm long section (measured from the top surface) of the stalagmite were collected at 20× and 50× magnification using a Zeiss Axiotech reflected light microscope with mercury vapour light source, and a black and white CCD camera, and analysed using Image Pro Plus/Express image analysis software. The distance between two consecutive luminescent laminae was measured from the centre position (e.g. peak intensity) of each individual lamina. Due to zones of less

massive calcite in the apex area of the stalagmite, the traverse for image analysis was positioned to the far right side of the sample slice (broken vertical line, Fig. 1c). The topmost 19 mm is dominated by closely spaced laminae and was re-counted twice after the initial analysis.

Powder for stable-isotope analysis was collected along the vertical growth axis at 0.5 mm intervals using a 0.5 mm dental drill (right slice, side view, Fig. 1d). More than 270 subsamples of 80–95 μg were analysed for stable oxygen and carbon isotopic composition. Subsamples were also measured at 1.5–10 mm intervals along three individual growth horizons (I–III, Fig. 3e and f) for isotopic equilibrium tests ('Hendy tests'). The analyses were done at the GMS Laboratory, University of Bergen, using a Finnigan MAT 251 mass spectrometer and an automatic on-line carbonate preparation device ('Kiel device'). Standard carbonate samples have an analytical 1σ uncertainty of ± 0.06 and $\pm 0.07\permil$, for $\delta^{13}C$ and $\delta^{18}O$ respectively. Results are reported as $\permil$ VPDB, using the NIST (NBS) 19 standard as a reference.

5. Results

5.1. TIMS U–Th dating

Fifteen TIMS analyses of the L-03 stalagmite (Table 1) reveal $[^{238}U]$ ranging from 2.8 to 5.8 $\mu g\,g^{-1}$, which is higher than commonly observed for Norwegian stalagmites (0.5–2.5 $\mu g\,g^{-1}$, e.g. Lauritzen, 1995; Lauritzen and Lundberg, 1999; Linge et al., 2001a,b; Berstad et al., 2002), variable $(^{234}U/^{238}U)_A$ from base to top, and high $[^{232}Th]$ ranging from 0.5 to 9.0 $\mu g\,g^{-1}$. The $(^{230}Th/^{232}Th)_A$ are all below 85, indicating that the ages must be corrected for a non-authigenic component of ^{230}Th. Except for the two uppermost analyses, all uncorrected ages are in chronostratigraphic order and are reported as years before AD 2000 with 2σ errors (Table 1, Fig. 2). When corrected for initial Th assuming an initial $^{230}Th/^{232}Th$ activity ratio $(^{230}Th/^{232}Th)_{A0}$, of 1.5 to be representative for detrital contamination (Schwarcz, 1980), all corrected ages are in chronostratigraphic order except analyses #335 and #305. The topmost corrected age is negative, showing that the applied correction factor used is not correct for this site or this part of the stalagmite. Regardless of contamination, the TIMS U–Th ages indicate that the stalagmite growth commenced before 3600 a, and terminated sometime after 700 a, but prior to being collected.

The upper limit $(^{230}Th/^{232}Th)_A$ for a sample to be considered relatively free from detrital contamination depends on the analytical precision of the measurement: previously, the criterion for alpha particle spectrometric analyses was set at $(^{230}Th/^{232}Th)_A > 20$ (e.g. Schwarcz, 1989), whereas Richards and Dorale (2003) and Hellstrom (2006) have suggested a ratio higher than 200 or 300 for mass-spectrometric measurements. Only 5 of the measurements in this study have $(^{230}Th/^{232}Th)_A > 20$ and all are <85, hence none of the measurements can be converted to age estimate without being corrected for initial ^{230}Th. It is not straightforward to establish a site- or sample-specific $(^{230}Th/^{232}Th)_{A0}$, or whether it has been constant over time (cf. Hellstrom, 2006). We have tentatively accepted the six 'most clean' analyses, i.e. those that displayed $[^{232}Th] < 800\,ng\,g^{-1}$ $(^{234}U/^{232}Th)_A$ above 1300, and $[^{238}U]/[^{232}Th] \geq 4$ (bold numbers, Table 1). This includes all but one analysis with $(^{230}Th/^{232}Th)_A > 15$. Based on the accepted analyses, we present four age models in Section 6.1. Two different tie-points were chosen for construction of age models because the impact of non-authigenic ^{230}Th on age calculations decreases with increasing age as ^{230}Th is produced in the crystal lattice. Age models 1 and 2 use TIMS analysis #323 (88.5 mm below top) as the tie-point, where model 1 uses the uncorrected U–Th age and model 2 the corrected U–Th age. Age models 3 and 4 use TIMS analysis #333 (8.5 mm below top) as the tie-point, where model 3 uses the uncorrected U–Th age and model 4 the corrected U–Th age.

5.2. Characteristics of luminescent lamination

Luminescent lamination is observed throughout the analysed interval (0–110.6 mm from top surface). Growth of the L-03 stalagmite is believed to have been continuous in this interval because no evidence of hiatuses is observed with a microscope. Two characteristic patterns of luminescence laminae are observed: 1) narrow zones with closely spaced and highly intense luminescent laminae (<20 μm between individual laminae, Fig. 3a, ii), which corresponding with white, visible bands in the stalagmite calcite, and 2) broader zones characterised by a repeating pattern of high-intensity luminescent lamina followed by up to 3 low-intensity laminae (Fig. 3a, i, iii and iv). Here, the distances between high to low-intensity laminae are typically 10–20 μm and 30–50 μm between low to high-intensity lamina, with typically 40–70 μm between two high-intensity laminae.
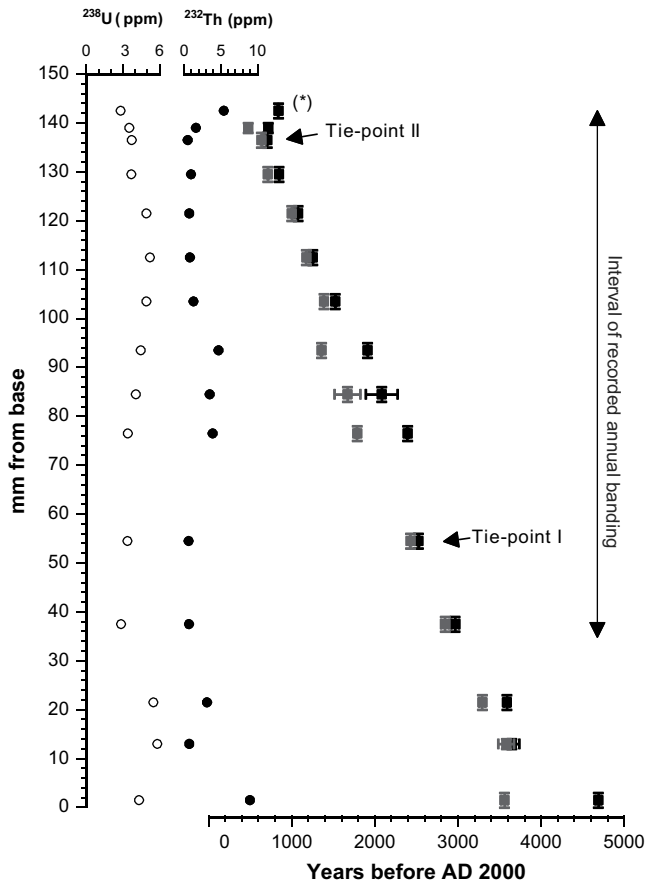
Table 1
Results from TIMS U–Th analyses of the L-03 stalagmite. Ages are in years before AD 2000 and errors are 2σ. All ratios are activity ratios. Bold numbers indicate analyses accepted after criteria used in Section 5.1.

Lab. no.	Position[a]	[b]	Band #	^{238}U (ng g^{-1})	^{232}Th (ng g^{-1})	$(^{234}U/^{238}U)_A$	$(^{230}Th/^{234}U)_A$	$(^{230}Th/^{232}Th)_A$	$(^{234}U/^{232}Th)_A$	Uncorrected Age $\pm 2\sigma$ (a)	Corrected Age $\pm 2\sigma$ (a)[c]
325	1.5 ± 1.5	2.0	137	2788 ± 3	5377	1.1155 ± 0.0034	0.0077 ± 0.0001	1.2 ± 0.1	157 ± 3	840 ± 11	−204 ± 14
337	5.0 ± 1.0	4.5	301	3516 ± 15	1559	1.1188 ± 0.0109	0.0066 ± 0.0001	4.5 ± 0.1	688 ± 9	715 ± 6	478 ± 6
333	**7.5 ± 1.5**	**8.5**	**439**	**3714 ± 2**	**486**	**1.1260 ± 0.0021**	**0.0065 ± 0.0001**	**15.2 ± 0.3**	**2346 ± 58**	**705 ± 12**	**636 ± 12**
324	14.5 ± 1.5	14.0	538	3670 ± 4	930	1.1349 ± 0.0038	0.0078 ± 0.0001	9.4 ± 0.1	1214 ± 14	848 ± 4	713 ± 5
304	**22.5 ± 1.5**	**24.5**	**818**	**4930 ± 6**	**690**	**1.1259 ± 0.0034**	**0.0098 ± 0.0001**	**21.9 ± 0.2**	**2229 ± 25**	**1075 ± 7**	**1001 ± 7**
336	**31.5 ± 1.5**	**31.5**	**989**	**5205 ± 7**	**766**	**1.1172 ± 0.0044**	**0.0115 ± 0.0001**	**23.7 ± 0.2**	**2065 ± 19**	**1253 ± 6**	**1174 ± 6**
335	40.5 ± 1.5	40.0	1175	4921 ± 5	1266	1.1206 ± 0.0035	0.0139 ± 0.0001	16.5 ± 0.2	1188 ± 13	1525 ± 10	1387 ± 11
305	50.5 ± 1.5	49.0	1356	4450 ± 7	4687	1.1273 ± 0.0039	0.0174 ± 0.0001	5.1 ± 0.1	294 ± 4	1912 ± 10	1357 ± 13
338	59.5 ± 1.5	58.0	1578	4046 ± 75	3478	1.2416 ± 0.1209	0.0190 ± 0.0017	7.5 ± 0.1	397 ± 36	2083 ± 190	1672 ± 157
306	67.5 ± 1.5	63.5	1644	3383 ± 4	3880	1.1296 ± 0.0036	0.0218 ± 0.0001	5.9 ± 0.1	271 ± 4	2392 ± 14	1787 ± 18
323	**89.5 ± 1.5**	**88.5**	**2255**	**3359 ± 4**	**601**	**1.1111 ± 0.0029**	**0.0230 ± 0.0001**	**38.6 ± 0.4**	**1683 ± 17**	**2525 ± 10**	**2428 ± 10**
339	109.5 ± 1.5	106.0	2693	2830 ± 10	647	1.1152 ± 0.0085	0.0269 ± 0.0004	35.7 ± 0.7	1326 ± 33	2967 ± 46	2844 ± 47
307	122.5 ± 1.5	–	–	5479 ± 12	3102	1.1249 ± 0.0066	0.0325 ± 0.0003	17.7 ± 0.2	546 ± 8	3590 ± 32	3291 ± 33
334	**131.0 ± 1.0**	**–**	**–**	**5755 ± 14**	**695**	**1.1132 ± 0.0067**	**0.0323 ± 0.0008**	**82.9 ± 2.8**	**2513 ± 107**	**3644 ± 93**	**3580 ± 94**
322	142 ± 1.5	–	–	4333 ± 7	8958	1.1040 ± 0.0045	0.0422 ± 0.0003	6.1 ± 0.1	145 ± 2	4689 ± 31	3560 ± 37

[a] Centre position in mm from top along TIMS/stable-isotope traverse.
[b] Corresponding centre position of TIMS subsamples in mm from top along luminescence traverse.
[c] Corrected assuming an initial $^{230}Th/^{232}Th$ activity ratio of 1.5 (Schwarcz, 1980).

Fig. 2. Variation in [^{238}U] (open circles) and [^{232}Th] (solid circles) from base (0 mm) to top (144 mm) of the L-03 stalagmite. Black squares represent uncorrected U–Th ages and grey squares represent U–Th ages corrected for a (^{230}Th/^{232}Th)$_{A0}$ of 1.5. Asterisk indicates a negative corrected age not displayed for the uppermost dated position (see Table 1). Error bars, where visible, are 2σ uncertainties.

A total of 3575 laminae were recorded, and no counting error has been assigned. Manual interpretation and layer-counting are subject to individual biases (Smith et al., 2009), but in this case the low-intensity laminae are much more likely to be overlooked than high-intensity laminae. Fig. 3b shows how the distance between consecutive laminae varies from the top surface and downwards. Because the bright, high-intensity laminae are present throughout the recorded interval, they are interpreted to represent annual deposition, whereas the low-intensity laminae may have been deposited sub-annually (cf. Tan et al., 2006). Fig. 3c shows the thickness variation of the interpreted 2783 annual bands from the top surface to the hiatus at ∼ 34 mm above sample base (0–110.6 mm from top). Annual band thickness varies from 2.4 to 106.5 μm, but is typically between 20 and 80 μm.

The luminescence ratio (Fig. 3d) is elevated at near-top and near-base of the stalagmite, as well as prior to the hiatus and at about 90 and 125 mm above base. A high ratio generally corresponds to zones of narrow band thickness; a low ratio does not appear to necessarily correlate to broader bands but rather to laminae frequency.

5.3. Testing the annual and sub-annual character

The interpretation of annual and sub-annual bands is tested by comparison with the TIMS U–Th chronology. Because the two chronologies originate from two separate traverses, the centre

position of each U–Th-dated subsample has been transferred and fixed on the luminescence traverse by tracing along the visible banding (see Table 1). The physical subsampling for U–Th dating represents the greatest source of uncertainty in this study: 2 mm vertical thickness of a Norwegian stalagmite sample commonly comprise between 20 and 200 years of calcite accretion (growth rates of 90–10 μm a^{-1}), hence inaccuracies in sampling and/or non-uniform growth rate may over- or underestimate the calculated age of the centre position. Table 2a shows that the interpreted annual banding compares well with the number of years between accepted U–Th dates regardless of whether the correction for detrital ^{230}Th is taken into account or not. The good correlation suggests that the uncertainty of the band counting is within errors of the ^{230}Th dates and that it is reasonable to infer annual banding. Both uncorrected and corrected ages support an annual nature of the banding without confirming either's correctness; consequently the banding record remains floating.

5.4. Stable isotopes

The so-called 'Hendy test' was performed along three distinct horizons (I–III from base to top, Fig. 3e–g). The internal variation in $\delta^{18}O_c$ and $\delta^{13}C_c$ (both in ‰ VPDB) is 0.28‰ and 0.08‰ for horizon I, 0.26‰ and 0.15‰ for horizon II, and 0.18‰ and 0.08‰ for horizon III (Fig. 3g). The correlation between $\delta^{18}O_c$ and $\delta^{13}C_c$ for each horizon is weak or non-existent, suggesting that the calcite was deposited in isotopic (quasi-) equilibrium with its dripwater. The large sample size and low-precision sampling (0.5 mm vs. ∼ 50 μm annual band thickness) should average out large variations and 'Hendy tests' performed this way are expected to always suggest equilibrium conditions for slow growing samples.

The variation in $\delta^{18}O_c$ and $\delta^{13}C_c$ from the base to the top of the sample is displayed in Fig. 3e and f, along with the positions of the three 'Hendy tested' layers. $\delta^{18}O_c$ values along the growth axis range from −7.20‰ to −8.17‰ VPDB (−8.30‰ with high standard deviation at 34.5 mm), and this is within the range found for other stalagmites (Holocene and Eemian) from the Rana area (Linge, 1999). $\delta^{13}C_c$ values range from −1.02‰ to −4.27‰ VPDB (−4.83‰ with high standard deviation at 34.5 mm); at the present, this data set displays the most enriched $\delta^{13}C_c$ values found for any stalagmite from northern Norway.

6. Discussion

6.1. Age models and initial ^{230}Th

Because of the generally high ^{232}Th levels in the L-03 stalagmite (Fig. 2), the main chronological challenge in this study is to maximise the accuracy where initial (^{230}Th/^{232}Th)$_{A0}$ activity is known. The relative effect of corrections for initial Th is much greater on young material such as this late Holocene sample. Table 2a shows that the banding chronology can be considered to be annual when the number of bands and number of years from U–Th ages are compared between dated positions.

Here we consider four age models based on different anchor points and ages for the floating annual band record (Table 2b). We have chosen two different tie-points (88.5 and 8.5 mm), where the U–Th dates are assumed to be accurate and based on a rationale declared below. The banding chronology is fixed in time by assigning an absolute age to the band corresponding to the centre position to the appropriate U–Th sample. For both tie-points, we present an uncorrected and a corrected age model. Tie-point I (88.5 mm from top, TIMS analysis #323, Table 1) provides a fixed point in time for models 1 and 2 (Figs. 2 and 4a, Table 2b), where model 1 uses the uncorrected U–Th age and model 2 the corrected
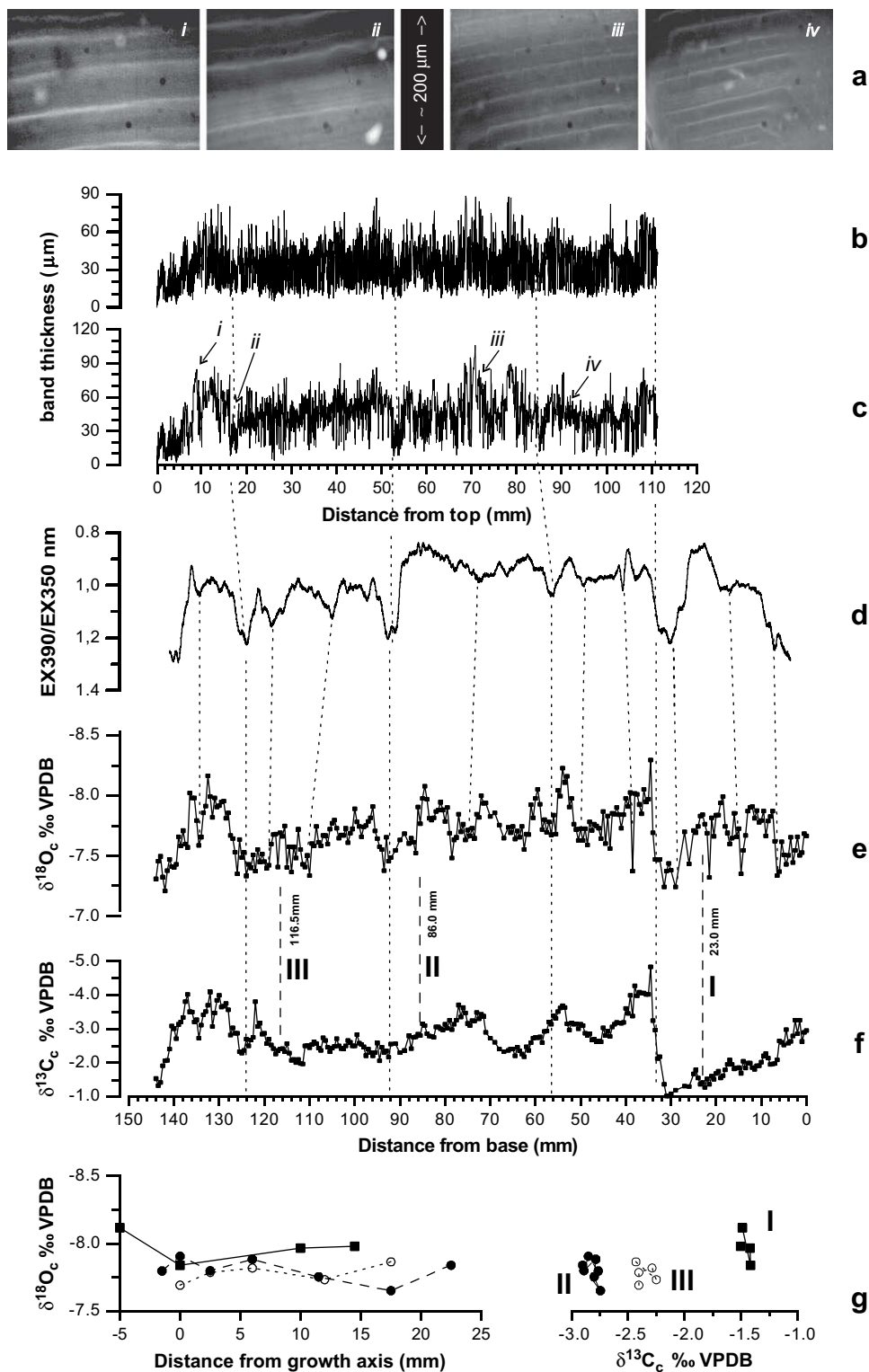
Fig. 3. a) Images of luminescent laminae: i) high-intensity laminae with intervening low-intensity laminae, ii) abrupt transition from narrow lamination to wide lamination, iii) medium-spaced lamination with transition to closely spaced lamination above, iv) variable spacing and multiple lamination. b) Distance in microns (μm) between consecutive luminescent laminae from the top surface of the stalagmite down to 110.6 mm (equals 34 mm above the base of the sample). c) Distance in microns (μm) between main annual luminescent laminae, i.e. the annual band thickness, from the top surface of the stalagmite and down to 110.6 mm. d) Luminescence ratio EX390/EX350 as a measure of humic/fulvic acid content and hence degree of decomposition in the soil zone. e) The stable oxygen isotope (‰ VPDB) stratigraphy from base (0 mm) to top (144 mm) along the vertical growth axis. Dotted, vertical lines correlate between corresponding features in records originating along separate traverses. Broken, vertical lines with roman numbers indicate the positions of the three layers where the 'Hendy test' was performed. f) The stable carbon isotope (‰ VPDB) stratigraphy from base (0 mm) to top (144 mm) along the vertical growth axis. g) Stable-isotope 'Hendy test' from layers I (solid line, solid square marker), II (grey, broken line, grey circles) and III (black, broken line, open circles). The left-hand panel shows the variation in $\delta^{18}O_c$ with distance from the vertical growth axis, whereas the right-hand panel shows the $\delta^{18}O_c$ values from each layer plotted against their corresponding $\delta^{13}C_c$ values.

Table 2a
Comparison of time intervals between accepted TIMS U–Th dates (uncorrected and corrected) with corresponding number of bands from the inferred annual banding record. Bold numbers indicate accepted analyses.

mm interval	Band interval	# of bands	Uncorrected years		Corrected years		# of bands between TIMS dates
			All dates[a]	Accepted[b]	All dates[a]	Accepted[b]	
0–2	**0**–137	137	n/a	n/a	n/a	n/a	439
2–4.5	137–301	164	-125 ± 13		682 ± 15		
4.5–8.5	301–**439**	138	-10 ± 13		158 ± 13		
8.5–14	**439**–538	99	143 ± 13	370 ± 14	77 ± 13	365 ± 16	379
14–24.5	538–**818**	280	227 ± 8		288 ± 9		
24.5–31.5	**818–989**	**171**	$\mathbf{178 \pm 9}$	$\mathbf{178 \pm 9}$	$\mathbf{173 \pm 9}$	$\mathbf{173 \pm 9}$	**171**
31.5–40	**989**–1175	186	272 ± 12	1272 ± 12	213 ± 17		
40–49	1175–1356	181	387 ± 14		-30 ± 19		
49–58	1356–1578	222	171 ± 190		315 ± 158	1254 ± 12	1266
58–60.5	1578–1644	66	309 ± 191		115 ± 158		
63.5–88.5	1644–**2255**	611	133 ± 17		641 ± 21		
88.5–106	**2255–2693**	**438**	$\mathbf{442 \pm 47}$	$\mathbf{442 \pm 47}$	$\mathbf{416 \pm 48}$	$\mathbf{416 \pm 48}$	**438**
106–110.57	2693–2783	90	n/a	n/a	n/a	n/a	n/a

[a] Difference in age between dated positions.
[b] Difference in age between accepted dates.

U–Th age. Tie-point I has the second lowest [^{232}Th] and the highest $(^{230}\text{Th}/^{232}\text{Th})_A$ of the analyses covering the luminescence traverse. Tie-point II (8.5 mm from top, TIMS analysis #333, Table 1) provides a fixed point in time for models 3 and 4, where model 3 uses the uncorrected U–Th age and model 4 the corrected U–Th age. Tie-point II has the lowest [^{232}Th] and the highest $(^{234}\text{U}/^{232}\text{Th})_A$, however, the $(^{230}\text{Th}/^{232}\text{Th})_A$ is only 15. Fig. 4a and b shows how age models 1–4 plot in relation to an ideal 1:1 relationship between annual banding ages and U–Th ages.

The deviation ($+$ or $-$) between model age and U–Th age is listed in Table 2b for each of the four fits. As expected, U–Th ages are greater than the annual band chronology ages (models 1 and 3) where measured $(^{230}\text{Th}/^{232}\text{Th})_A$ is $< \sim 20$ (Table 2b). This is attributed the presence of non-authigenic ^{230}Th. The corrected U–Th ages lie either side of the 1:1 relationship for model 2, and are generally younger for model 4, suggesting both under- and

overcorrection when assuming a $(^{230}\text{Th}/^{232}\text{Th})_{A0} = 1.5$. The maximum difference between all four models is 97 a for the upper growth band of the stalagmite.

To obtain a perfect fit between the U–Th dates and the model ages, one can allow $(^{230}\text{Th}/^{232}\text{Th})_{A0}$ to vary. By using the $(^{234}\text{U}/^{238}\text{U})_A$ and $(^{230}\text{Th}/^{234}\text{U})_A$ from Table 2b, we have estimated the subsample-specific $(^{230}\text{Th}/^{232}\text{Th})_{A0}$ required to produce the ages suggested by the age models (Table 2b), declared as 'forced ages' in Table 3. The tie-point in each age model should then obtain a $(^{230}\text{Th}/^{232}\text{Th})_{A0}$ equal to the correction factor used, i.e. 0 (models 1 and 3), and 1.5 (models 2 and 4). Negative $(^{230}\text{Th}/^{232}\text{Th})_{A0}$ cannot be supported, and must be attributed to counting error or, more likely, reflect the uncertainty associated with attaching the U–Th subsamples on an annual banding scale (see Section 5.3).

Assuming that the U–Th ages for the anchor positions are accurate, $(^{230}\text{Th}/^{232}\text{Th})_{A0}$ for models 1 and 3 are found to vary

Table 2b
Comparison of age models based on annual banding data with the uncorrected and corrected TIMS U–Th data. Bold numbers under 'raw data' indicate accepted analyses; bold numbers under 'age models' indicate anchor points.

Raw data (Table 1)						Age models ($+/-$ deviation from TIMS ages)[b]			
Lab. no.	Position (mm from surface)[a]	$(^{230}\text{Th}/^{232}\text{Th})_A$	$(^{234}\text{U}/^{232}\text{Th})_A$	TIMS uncorrected Age $\pm 2\sigma$ (a)	TIMS corrected Age $\pm 2\sigma$ (a)	Model 1 (AD 1729)[c] (oldest)	Model 2 (AD 1826)[d] (youngest)	Model 3 (AD 1733)[e]	Model 4 (AD 1802)[f]
–	0.0024	–	–	–	–	271	174	267	198
325	2.0	1.2 ± 0.1	157 ± 3	840 ± 11	-204 ± 14	407 (-433)	310 ($+514$)	403 (-437)	334 ($+538$)
337	4.5	4.5 ± 0.1	688 ± 9	715 ± 6	478 ± 6	571 (-144)	474 (-4)	567 (-148)	498 ($+20$)
333	**8.5**	$\mathbf{15.2 \pm 0.3}$	$\mathbf{2346 \pm 58}$	$\mathbf{705 \pm 12}$	$\mathbf{636 \pm 12}$	709 ($+4$)	612 (-24)	**705 (0)**	**636 (0)**
324	14.0	9.4 ± 0.1	1214 ± 14	848 ± 4	713 ± 5	808 (-40)	711 (-2)	804 (-44)	735 ($+22$)
304	**24.5**	$\mathbf{21.9 \pm 0.2}$	$\mathbf{2229 \pm 25}$	$\mathbf{1075 \pm 7}$	$\mathbf{1001 \pm 7}$	1088 ($+13$)	991 (-10)	1084 ($+9$)	1015 ($+14$)
336	**31.5**	$\mathbf{23.7 \pm 0.2}$	$\mathbf{2065 \pm 19}$	$\mathbf{1253 \pm 6}$	$\mathbf{1174 \pm 6}$	1259 ($+6$)	1162 (-12)	1255 ($+2$)	1186 ($+12$)
335	40.0	16.5 ± 0.2	1188 ± 13	1525 ± 10	1387 ± 11	1445 (-80)	1348 (-39)	1441 (-84)	1372 (-15)
305	49.0	5.1 ± 0.1	294 ± 4	1912 ± 10	1357 ± 13	1626 (-286)	1529 ($+172$)	1622 (-290)	1553 ($+197$)
338	58.0	7.5 ± 0.1	397 ± 36	2083 ± 190	1672 ± 157	1848 (-235)	1751 ($+79$)	1844 (-239)	1775 ($+103$)
306	63.5	5.9 ± 0.1	271 ± 4	2392 ± 14	1787 ± 18	1914 (-478)	1817 ($+30$)	1910 (-482)	1841 ($+54$)
323	**88.5**	$\mathbf{38.6 \pm 0.4}$	$\mathbf{1683 \pm 17}$	$\mathbf{2525 \pm 10}$	$\mathbf{2428 \pm 10}$	2525 (0)	2428 (0)	2521 (-4)	2452 ($+24$)
339	**106.0**	$\mathbf{35.7 \pm 0.7}$	$\mathbf{1326 \pm 33}$	$\mathbf{2967 \pm 46}$	$\mathbf{2844 \pm 47}$	2963 (-4)	2866 ($+22$)	2959 (-8)	2890 ($+46$)
307	–	17.7 ± 0.2	546 ± 8	3590 ± 32	3291 ± 33	–	–	–	–
334	–	$\mathbf{82.9 \pm 2.8}$	$\mathbf{2513 \pm 107}$	$\mathbf{3644 \pm 93}$	$\mathbf{3580 \pm 94}$	–	–	–	–
322	–	6.1 ± 0.1	145 ± 2	4689 ± 31	3560 ± 37	–	–	–	–

[a] Centre position of TIMS subsample on luminescence traverse, in mm from top of stalagmite.
[b] Age models 1–4 with their suggested year of growth termination. ($+/-$) denotes the offset of the age model compared to the U–Th dates.
[c] Tie-point between the two chronologies chosen at 88.5 mm because of best ^{230}Th/^{232}Th activity ratio value, anchor point (bold) is an uncorrected U–Th age.
[d] Tie-point between the two chronologies chosen at 88.5 mm because of best ^{230}Th/^{232}Th activity ratio value, anchor point (bold) is a corrected U–Th age.
[e] Tie-point between the two chronologies chosen at 8.5 mm because of best ^{234}U/^{232}Th activity ratio value, anchor point (bold) is an uncorrected U–Th age.
[f] Tie-point between the two chronologies chosen at 8.5 mm because of best ^{234}U/^{232}Th activity ratio value, anchor point (bold) is a corrected TIMS age.
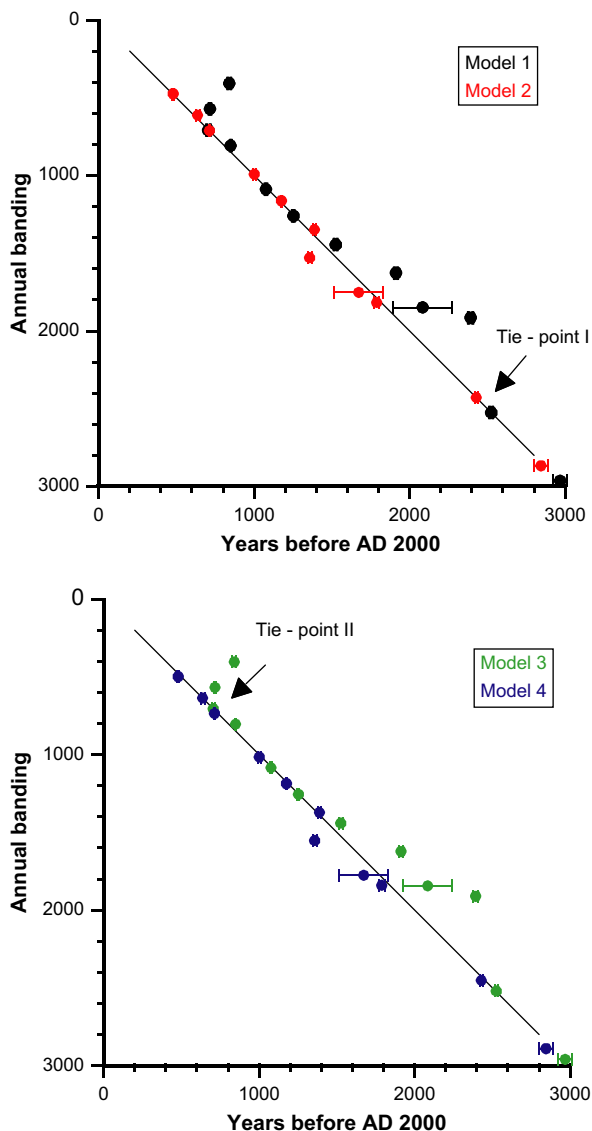
Fig. 4. Annual banding vs. U–Th chronology from Table 2b. The solid line indicates a 1:1 correspondence between the U–Th chronology and the annual band chronology. a) Age models 1 and 2 were constructed by tying the annual band chronology (Table 2a) to the U–Th age at 88.5 mm, uncorrected for model 1 and corrected value for model 2, and using the number of annual bands between dated positions to obtain alternative ages to U–Th ages (Table 2b). b) Age models 3 and 4 were constructed by tying the annual banding chronology to the U–Th age at 8.5 mm, uncorrected value for model 3 and corrected value for model 4, and using the number of annual bands between dated positions to obtain alternative ages to U–Th ages (Table 2b).

between 1.20 and -0.28, with average values of 0.44 ± 0.73 and 0.48 ± 0.70, respectively. Similarly, assuming that the U–Th ages for the anchor positions are accurate when corrected for an initial activity ratio of 1.5 $(^{230}\text{Th}/^{232}\text{Th})_{A0}$ for models 2 and 4 are found to vary between 0.72 and 2.03, with average values of 1.47 ± 0.63 and 1.21 ± 0.47, respectively. This exercise shows that for each age model the average $(^{230}\text{Th}/^{232}\text{Th})_{A0}$ disguise a broad range of sample-specific values (Table 3) and do not appear representative for typical ratios.

Of all the age models, model 4 is the one with the least spread in $(^{230}\text{Th}/^{232}\text{Th})_{A0}$ (Table 3), suggesting that the average estimate of 1.21 ± 0.47 is better than the applied one of 1.5. This supports the deviations noted when comparing the difference between age model 4 and corrected U–Th ages. Despite this, we have chosen to use age model 2 for our band thickness data. A more uniform

$(^{230}\text{Th}/^{232}\text{Th})_{A0}$ is not necessarily more correct than variable values. Moreover, the older tie-point is believed to be the least affected by contamination as the proportion of non-authigenic vs. radiogenic ^{230}Th diminishes with time. According to age model 2 the average $(^{230}\text{Th}/^{232}\text{Th})_{A0}$ required to force U–Th ages to correspond with banding ages is 1.47 ± 0.63 (Table 3). This is close to the conventionally used value of 1.5 (Schwarcz, 1980), and suggests that using the corrected U–Th age for the tie-point is plausible, although not necessarily correct.

Our findings confirm that (1) knowledge of the $(^{230}\text{Th}/^{232}\text{Th})_{A0}$ is crucial for accurate U–Th age determinations on young samples (e.g. Richards and Dorale, 2003), (2) even with this knowledge, an uncertainty is introduced because this ratio can vary through time (e.g. Richards and Dorale, 2003), and (3) the combination of annual laminae and high-precision U–Th dating provides the best method of constraining the age of young stalagmite samples, and of producing age models for high-resolution (micro-milled) stable isotope and/or trace element records.

6.2. Interpretation of luminescence properties and growth rate variations

The luminescence ratio does not have proper age control (see Section 4). From comparison with the annual banding (Fig. 3d) the pattern of luminescence ratio mimics that of the growth rate. Intervals of high EX390/EX350 are correlated with brief intervals of condensed growth, an identical observation to that observed in the peat overlain site of Uamh an Tartair, northwest Scotland (Proctor et al., 2000). The luminescence ratio (either EX390/EX350 as utilised here, or similar wavelength ratios in the long wavelength UV/blue) has previously been used as a measure of the organic matter character (e.g. McGarry and Baker, 2000; Proctor et al., 2000; Perrette et al., 2005; Asrat et al., 2007) and in particular the degree of decomposition in the soil zone. A relative high luminescence ratio EX390/EX350, i.e. a greater proportion high molecular weight/more aromatic material, can therefore be interpreted as indicating cooler and wetter conditions, whereas relatively low luminescence ratios are indicative of warmer and drier conditions. We interpret the luminescence ratio to be biased towards reflecting summer conditions because of low soil activity during winter.

The variability in number of luminescent laminae displayed per year (Fig. 5b) show overall more laminae per year during intervals with low luminescence ratio. The multiple laminae pattern can be hypothesised to reflect the hydrological seasonal variation in northern Norway, as characterised by snowmelt/ice break-up in the spring and variable rainstorms and floods in the autumn (e.g. Johannessen, 1970).

The annual growth rate varies between 2 and 107 μm a^{-1}, and for the full 2783-year record the average is close to 40 μm a^{-1}. In the 11-year running mean curve (Fig. 5a), periods of relatively high (>40 μm a^{-1}) and low (<40 μm a^{-1}) growth rate can be discerned. High (>25 μm a^{-1}) and low (<25 μm a^{-1}) amplitude shifts can also be identified. The high amplitude shifts need not reflect rapid climate changes, but could instead reflect a non-linear response of growth rate to surface climate (available humidity, soil production, etc.).

Condensed growth and high luminescence ratio can be taken to reflect overall cool/wet conditions with a lesser degree of decomposition of organic matter, whereas thicker bands and low luminescence ratio reflect milder/drier conditions. We therefore interpret the low luminescence ratio, the multiple laminae and thick bands to reflect years with milder/drier summer conditions.

From the top surface and back in time, the luminescence-derived data is described with reference to age model 2, and is grouped in four periods (Table 4) characterised by average trends in

Table 3
Individual and average ^{230}Th/^{232}Th$_{A0}$ for TIMS analyses. The values are estimated from the measured activity ratios (see Table 1) and the ages predicted using age models 1–4.

Lab. no.	Measured			Model 1		Model 2		Model 3		Model 4	
	$(^{234}$U/^{238}U$)_A$	$(^{230}$Th/^{234}U$)_A$	$(^{230}$Th/^{232}Th$)_A$	Forced age[b]	Est. ratio[c]	Forced age[b]	Est. ratio[c]	Forced age[b]	Est. ratio[c]	Forced age[b]	Est. ratio[c]
325	1.1155	0.00769	1.2	407	0.62	310	0.76	403	0.63	334	0.72
337	1.1188	0.00656	4.5	571	0.91	474	1.52	567	0.94	498	1.37
333[a]	1.1260	0.00647	**15.2**	709	−0.07	612	2.03	**705**	**0.02**	**636**	**1.51**
324	1.1349	0.00777	9.4	808	0.45	711	1.53	804	0.49	735	1.26
304[a]	1.1259	0.00983	21.9	1088	−0.28	991	1.70	1084	−0.20	1015	1.21
336[a]	1.1172	0.01146	23.7	1259	−0.11	1162	1.74	1255	−0.03	1186	1.28
335	1.1206	0.01392	16.5	1445	0.86	1348	1.92	1441	0.91	1372	1.66
305	1.1273	0.01743	5.1	1626	0.77	1529	1.03	1622	0.78	1553	0.96
338	1.2416	0.01898	7.5	1848	0.85	1751	1.21	1844	0.87	1775	1.12
306	1.1296	0.02176	5.9	1914	1.19	1817	1.43	1910	1.20	1841	1.37
323[a]	1.1111	0.02296	**38.6**	2525	**0.00**	2428	**1.50**	2521	0.07	2452	1.13
339[a]	1.1152	0.02692	35.7	2963	0.04	2866	1.23	2959	0.10	2890	0.93
Average ^{230}Th/^{232}Th$_{A0}$					**0.44**		**1.47**		**0.48**		**1.21**
					−0.72		−0.71		−0.68		−0.49
					+0.75		+0.56		+0.72		+0.45

[a] Accepted TIMS dates.
[b] Forced age: age obtained using the annual banding record and one anchor point, see Table 2a and 2b.
[c] Initial activity ratio of ^{230}Th/^{232}Th required forcing the U–Th age to that predicted from number of intense luminescent laminae between dated positions.

growth rate, laminae frequency and luminescence ratio. Conditions apparently unfavourable for stalagmite growth occur for brief intervals (<100 a), whereas favourable conditions persist for longer intervals (>500 a). An exception to this is the most recent IV: here overall high growth rate lasted about 150 years before becoming very subdued for more than 400 years, and finally terminate.

6.3. Interpretation of the stable-isotope data

Because cave dripwater is part of the meteorological cycle, changes in δ^{18}O$_c$ can be attributed to changing conditions from water source to surface of the stalagmite. Information pertinent to the cave and/or surface conditions during stalagmite growth can be obtained from relative changes in the stable oxygen and carbon isotope composition of the calcite (e.g. Fairchild et al., 2006). Earlier work from northern Norway on Holocene stalagmites show a negative relationship between δ^{18}O$_c$ and temperature (Lauritzen and Lundberg, 1999; Linge, 1999; Linge et al., 2001b), and the same is inferred for the L-03 stalagmite based on the δ^{18}O$_c$ pattern the most recent ca. 600 years of the record. This relationship is consistent with the temperature-dependent fractionation constant between calcite and water (O'Neil et al., 1969), but opposes the positive correlation between temperature and δ^{18}O values of meteoric precipitation.

Seasonality can explain the observed negative correlation between δ^{18}O$_c$ and temperature at high latitudes by causing selective infiltration of seepage water and hence modifying the isotopic composition of cave dripwaters. Prolonged conditions with frozen ground may filter away the winter water by surface run-off or evaporation in spring causing δ^{18}O values in cave dripwaters to be biased towards summer conditions. In addition, cooler summers would reduce evapotranspiration and could allow more heavy summer water into the aquifer. On the other hand, milder years will allow a larger fraction of winter water to percolate, hence resulting in overall lower δ^{18}O values in dripwater, closer to the annual average of the meteoric precipitation at the location.

Similarly, the contrast between soil zone conditions during the vegetation growth season and the snow-covered season will lead to a large seasonal isotopic variation in stable carbon isotopes of the percolating waters. Soil CO_2 has a strong seasonal variation in regions with distinct seasonal changes in temperature and precipitation (e.g. Dyer and Brook, 1991; Hamada and Tanaka, 2001; Spötl et al., 2005). An inverse relationship exists between soil–δ^{13}C

and soil–pCO_2 (Rightmire, 1978; Hesterberg and Siegenthaler, 1991) implying that under high-pCO_2 conditions the δ^{13}C of soil–CO_2 approaches the δ^{13}C value of the dominant vegetation (photosynthetic pathway dependant) (Cerling et al., 1991). Soil water is therefore expected to have more depleted δ^{13}C values during summer than during winter. Depleted δ^{13}C$_c$ values in stalagmites in northern Norway are hence thought to reflect mild/dry conditions.

Tentative tuning of the stable-isotope record to the annual banding record, by tracing along visible bands between the two traverses, produces an improved visible fit with the annual banding record (Fig. 5h and j). An even better fit might be expected if tracing of visible bands were conducted using a microscope. However, we consider that this would only be appropriate if stable-isotope sampling was done by micro-milling. A caveat when comparing annual growth rate variation and stable-isotope records is the marked difference in temporal resolution and dating accuracy. The stable-isotope record is composed of measurements averaging every 0.5 mm, whereas TIMS-samples commonly integrate over more years than the indicated by the 2σ dating uncertainty. In addition, the TIMS and stable-isotope records from the L-03 stalagmite originate from a separate traverse from the banding chronology, and correlation between the two traverses represents a source of reduced precision and accuracy.

The overall trends in the stable-isotope data, according to the tuned age model, are interpreted (Table 4) for the same four periods as the luminescence data for comparison. Single measurements show 'noise' due to shifting signature of the dripwater (10–40 a average values) reflecting variable surface conditions and/or isotopic composition of the meteoric precipitation. The longer-term changes in stable-isotope signature can be linked to the impact shifting surface conditions have on the cave environment, where the cave environment averages the surface conditions over time spans related to cave ventilation, roof thickness and water transport.

6.4. Inferred palaeoclimate record from the L-03 stalagmite

We use the luminescence ratio, annual band frequency, relative growth rate and stable isotopic composition to evaluate possible palaeoclimate signals (Table 4). The only available information about the prevailing conditions during the period of stalagmite growth is that determined from the measured proxy data, and we have applied a multiple parameter approach to best determine the
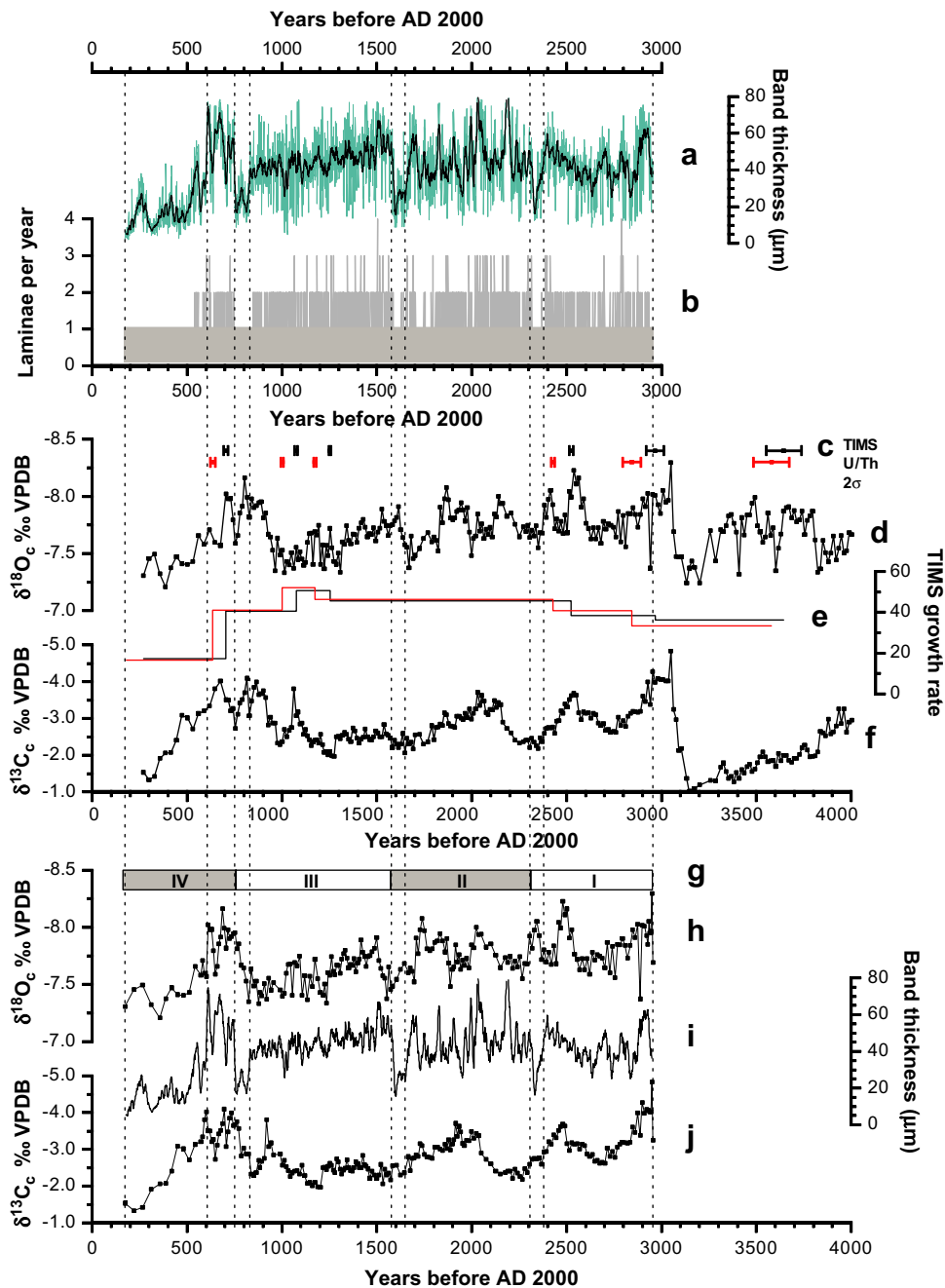
Fig. 5. a) The variation in band thickness/growth rate with time. The grey/light blue curve displays the thickness of the annual bands while the smoothed, black curve is an 11-years running mean of the annual data. The age of the youngest band is 174 years (AD 1826) and the age of the oldest band is 2956 years (956 BC). b) The number of luminescent laminae per year in the time period from 174 to 2956 years before AD 2000. Note that during the last ∼400 years of the record only one lamina is deposited per year and that intervals of narrow band thickness (low growth rate) tend to correspond with periods of single-lamina years. c) Position in time for uncorrected (black) and corrected (red) U–Th ages, corresponding to the two age models in e. d) Stable oxygen isotope stratigraphy with time, age model based on linear growth rates between U–Th-dated positions (corrected dates, see discussion section for elaboration). e) Two growth models based on linear interpolation between dated positions; uncorrected (black), corrected (red). f) Stable carbon isotope stratigraphy with time, age model based on linear growth rates between U–Th-dated positions (corrected dates, see discussion section for elaboration). g) Four periods (I–IV) showing gradual decrease in growth rate and culminating in very low rates. h) $\delta^{18}O_c$ tuned to annual banding curve (visual correlation of bands between the luminescent banding and stable-isotope transects, Fig. 1c and d). i) 11-year running mean annual band thickness variation. j) $\delta^{13}C_c$ curve tuned to annual banding curve (visual correlation of bands between the luminescent banding and stable-isotope transects, Fig. 1c and d). (For interpretation of the references to colour in this figure legend, the reader is referred to the web version of this article.)

underlying climate forcing (cf. Asrat et al., 2007). This is not without caveats; in addition to the complexity of individual proxies, the luminescent laminae occur at sub-annual frequency while stable-isotope variation in dripwater as monitored in caves (Lauritzen and Lundberg, 1999) do not display the strong seasonal variation as observed in the surface. Therefore, the reservoir characteristics of stable isotopes and organic matter are different, suggesting that the water itself has a residence time long enough to smooth the annual signal, whereas the organic concentration in the dripwater is a wash-out effect governed by discharge and not by the residence time of water. The stable-isotope signal, albeit dampened, is then a proxy for precipitation values (temperature of source and surface)

Table 4
Paleoclimate information inferred from proxy data from the L-03 stalagmite.

Period	Time interval		Growth rate/luminescence ratio/laminae frequency	$\delta^{18}O$	$\delta^{13}C$	Prevailing climatic conditions
	Years before AD 2000	AD/BC				
IV	~175–600	AD 1825–1400	Cool/short summer	Cooling	Cool/wetter	Cool Wet, short summer
	~600–750	AD 1400–1250	Mild/long summer	Mild	Mild/drier	Mild Long summer season
III	~760–825	AD 1240–1175	Cool/short summer	Less mild	Cool/drier	Cool Short summer season
	~850–1575	AD 1150–425	Mild/long summer	Mild to less mild	Mild	Mild, but gradually cooler/shorter summers
II	~1575–1650	AD 425–350	Mild/long summer	Cool	Mild/wetter	Cool Short summer season
	~1650–2300	AD 350–300 BC	Mild/long summer	Mild	Mild/wetter	Mild Long summer season
I	~2310–2375	310–375 BC	Cool/short summer	Mild	Mild/wetter	Cool Short summer season
	~2375–2955	375–955 BC	Mild/long summer	Mild	Mild/wetter	Mild Long summer season

as well as quantity (amount percolated), whereas the luminescent banding is a direct proxy of precipitation quantity and/or frequency.

The interpreted palaeoclimate from the L-03 proxy data is summarised in Table 4. Comparing the individual proxy records tentatively derives the prevailing climatic conditions within each period, as individual records and/or proxies rarely provide unambiguous indications. Ambiguities arise as the proxy properties are connected to both surficial and cave processes. The large-scale development in climatic conditions from the hiatus (>2950 a) to the cessation of growth (<300 a) can be described as four periods (Fig. 5g), each comprising a relative transition from high to low growth rate. Each period culminates in an interval of condensed growth, and these intervals are of increased duration towards the top of the stalagmite. For the oldest period I the longer trend differs slightly from the general description. Periods II and IV display larger variation than period III. This is interpreted to reflect gradually cooler and/or shorter summers within each period culminating in cessation of growth during or towards the end of LIA. Termination of stalagmite growth is suggested to have occurred between AD 1729 and 1826, and may, for instance, be linked either to climate deterioration and/or to local alterations in the percolation pathway.

Climate deterioration during the LIA would most likely have been manifested as repeated years with prolonged frozen ground conditions during autumn, winter and spring and low biological production during summer. Even minor slope processes at the surface, caused by the combination of repeated/prolonged deep frost and wet/cool summers, could cause alteration or inactivation of percolation pathways by blocking or infill.

A similar alteration in the infiltration zone could be associated with the $M_s \sim 6$ earthquake in AD 1819, or that the quake simply led to termination of stalagmite growth due to displacement of the drip source. A seven-year discrepancy between growth termination (model 2) and quake might either show the uncertainty in the age model, or reflect a true time lag.

Although of substantially lower resolution, the stable oxygen isotope data (Fig. 5h) show an overall increase from the hiatus towards the top of the sample. This can be taken as reflecting 1) warming of the source water, 2) shortening of the growth season (preventing percolation of winter water), or 3) cooling of the cave air temperature (i.e. annual average temperature at the surface). Reduced growth season and reduced mean annual temperature can be connected and is supported both the growth rate pattern and the record of laminae frequency. Likewise, the stable carbon isotope signal shows an overall increase with decreasing age (Fig. 5j),

suggesting a shortening of the duration of high soil activity or an overall reduction in soil activity. This can be linked to both decreased surface temperature and increased humidity (soil water and/or drip rate).

7. Conclusions

1) A 2783-year long, floating record of annual growth rate variation is constructed from luminescent lamination in a stalagmite from Rana, northern Norway. Four age models are proposed to anchor the annual growth rate record in time. The preferred model is based on tying the U–Th and annual chronologies together at the position of the most robust U–Th date (88.5 mm from the top) and using the corrected U–Th age. From this it is proposed that the stalagmite growth terminated at AD 1826, and that the termination can be linked to climate deterioration during the LIA and/or to local alterations in the percolation pathway after an $M_s \sim 6$ earthquake in AD 1819.

2) In order to obtain a good match between the U–Th dates and the model ages the $(^{230}Th/^{232}Th)_{A0}$ must be allowed to vary. Assuming that the U–Th ages for the anchor positions are accurate, average $(^{230}Th/^{232}Th)_{A0}$ for models 1 and 3 are 0.44 ± 0.73 and 0.48 ± 0.70, respectively. Similarly, assuming that the U–Th ages for the anchor positions are accurate when corrected for an initial activity ratio of 1.5, average $(^{230}Th/^{232}Th)_{A0}$ for models 2 and 4 are 1.47 ± 0.63 and 1.21 ± 0.47, respectively. The values obtained on individual samples largely differ from the average values, dissuading the use of one fixed correction factor when working on young stalagmites, and suggesting that the combination of annual laminae and high-precision U–Th dating provides the best method of constraining the age of young stalagmite samples.

3) Complementary stable-isotope data mirrors the large-scale changes in the growth rate curve. Despite substantial differences in temporal resolution, the combined information from growth rate (including laminae frequency and luminescence ratio) and stable-isotope data can be used to reconstruct a palaeoclimate record. The growth rate and luminescence characteristics are believed to predominantly reflect surface summer conditions, whereas the stable oxygen isotope and stable carbon records are more complex. The proxy data from L-03 is interpreted to show a gradual cooling and/or shortening of the vegetation growth season for the last 3000 years.

Acknowledgements

Editorial handling by: D. Richards

References

Asrat, A., Baker, A., Umer Mohammed, M., Leng, M.J., Van Calsteren, P., Smith, C., 2007. A high-resolution multi-proxy stalagmite record from Mechara, Southeastern Ethiopia: palaeohydrological implications for speleothem palaeoclimate reconstruction. Journal of Quaternary Science 22, 53–63.

Aune, B., 1993. Årstider og vekstsesong (Seasons of the year and growth season) 1:7 mill Nasjonalatlas for Norge. Statens kartverk. pp.

Baker, A., Genty, D., Dreybrodt, W., Barnes, W.L., Mockler, N.J., Grapes, J., 1998. Testing theoretically predicted stalagmite growth rate with recent annually laminated samples: implications for past stalagmite deposition. Geochimica et Cosmochimica Acta 62, 393–404.

Baker, A., Proctor, C.J., Barnes, W.L., 1999. Variations in stalagmite luminescence laminae structure at Poole's Cavern, England, AD 1910–1996: calibration of a palaeoprecipitation proxy. The Holocene 9, 683–688.

Baker, A., Proctor, C.J., Barnes, W.L., 2002. Stalagmite lamina doublets: a 1000 year proxy record of severe winters in northwest Scotland. International Journal of Climatology 22, 1339–1345.

Baker, A., Smart, P.L., Edwards, R.L., Richards, D.A., 1993. Annual growth banding in a cave stalagmite. Nature 364, 518–520.

Berstad, I.M., Lundberg, J., Lauritzen, S.-E., Linge, H., 2002. Comparison of the climate during marine isotope stage 9 and 11 inferred from a speleothem isotope record from northern Norway. Quaternary Research 58, 361–371.

Bourdon, B., Turner, S., Henderson, G.M., Lundstrom, C.C., 2003. Introduction to U-series geochemistry. Reviews in Mineralogy and Geochemistry 52, 1–22.

Broecker, W.A., Olson, E.A., Orr, P.C., 1960. Radiocarbon measurements and annual rings in cave formations. Nature 185, 93–94.

Cerling, T.E., Solomon, D.K., Quade, J., Bowman, J.R., 1991. On the isotopic composition of carbon in soil carbon dioxide. Geochimica et Cosmochimica Acta 55, 3403–3405.

Dreybrodt, W., 1999. Chemical kinetics, speleothem growth and climate. Boreas 28, 347–356.

Dyer, J.M., Brook, G.A., 1991. Spatial and temporal variations in temperate forest soil carbon dioxide during the non-growing season. Earth Surface Processes and Landforms 16, 411–426.

Edwards, R.L., Chen, J.H., Wasserburg, G.J., 1987. ^{238}U–^{234}U–^{230}Th–^{232}Th systematics and the precise measurement of time over the past 500,000 years. Earth and Planetary Science Letters 81, 175–192.

Fairchild, I.J., Smith, C.L., Baker, A., Fuller, L., Spötl, C., Mattey, D., McDermott, F.E.I.M.F., 2006. Modification and preservation of environmental signals in speleothems. Earth-Science Reviews 75, 105–153.

Gascoyne, M., 1992. Palaeoclimate determination from cave calcite deposits. Quaternary Science Reviews 11, 609–632.

Genty, D., Quinif, Y., 1996. Annually laminated sequences in the internal structure of some Belgian stalagmites – importance for paleoclimatology. Journal of Sedimentary Research 66, 275–288.

Goldstein, S.J., Stirling, C.H., 2003. Techniques for measuring uranium-series nuclides: 1992–2002. Reviews in Mineralogy and Geochemistry 52, 23–57.

Hamada, Y., Tanaka, T., 2001. Dynamics of carbon dioxide in soil profiles based on long-term field observations. Hydrological Processes 15, 1829–1845.

Hellstrom, J., 2006. U–Th dating of speleothems with high initial ^{230}Th using stratigraphical constraint. Quaternary Geochronology 1, 289–295.

Hesterberg, R., Siegenthaler, U., 1991. Production and stable isotopic composition of CO_2 in a soil near Bern, Switzerland. Tellus 43B, 197–205.

Hicks, E.C., Bungum, H., Lindholm, C.D., 2000. Seismic activity, inferred crustal stresses and seismotectonics in the Rana region, northern Norway. Quaternary Science Reviews 19, 1423–1436.

Ivanovich, M., Harmon, R.S., 1992. Uranium-series Disequilibrium: Applications to Earth, Marine, and Environmental Sciences. Clarendon Press, Oxford, 910 pp.

Johannessen, T.W., 1970. The climate of Scandinavia. In: Wallén, C.C. (Ed.), Climates of Northern and Western Europe. World Survey of Climatology. Elsevier, Amsterdam, pp. 23–79.

Jones, P.D., Briffa, K.R., Osborn, T.J., Lough, J.M., van Ommen, T.D., Vinther, B.M., Luterbacher, J., Wahl, E.R., Zwiers, F.W., Mann, M.E., Schmidt, G.A., Ammann, C.M., Buckley, B.M., Cobb, K.M., Kull, C., Küttel, M., Mosley-Thompson, E., Overpeck, J.T., Riedwyl, N., Schulz, M., Thudhope, A.W., Villalba, R., Wanner, H., Wolff, E., Xoplaki, E., 2009. High-resolution palaeoclimatology of the last millennium: a review of current status and future prospects. The Holocene 19, 3–49.

Kaufmann, G., Dreybrodt, W., 2004. Stalagmite growth and palaeo-climate: an inverse approach. Earth and Planetary Science Letters 224, 529–545.

Lauritzen, S.-E., 1991a. Uranium series dating of speleothems: a glacial chronology for Nordland; Norway, for the last 600 ka. Striae 34, 127–133.

Lauritzen, S.-E., 1991b. Karst resources and their conservation in Norway. Norsk Geografisk Tidsskrift 45, 119–142.

Lauritzen, S.-E., 1995. High-resolution paleotemperature proxy record for the Last Interglaciation based on Norwegian speleothems. Quaternary Research 43, 133–146.

Lauritzen, S.-E., 2003. Reconstructing Holocene climate records from speleothems. In: Mackay, A., Battarbee, R., Birks, J., Oldfield, F. (Eds.), Global Change in the Holocene. Hodder Arnold, London, pp. 242–263.

Lauritzen, S.-E., Løvlie, R., Moe, D., Østbye, E., 1990. Paleoclimate deduced from a multidisciplinary study of a half-million-year-old stalagmite from Rana, Northern Norway. Quaternary Research 34, 306–316.

Lauritzen, S.-E., Lundberg, J., 1999. Calibration of the speleothem delta function: an absolute temperature record for the Holocene in northern Norway. The Holocene 9, 659–669.

Linge, H., 1999. Isotopic Studies of some Northern Norwegian Speleothems and Calcareous Algae from Svalbard. Unpublished Ph.D. thesis, University of Bergen, Bergen, 83 pp.

Linge, H., Lauritzen, S.-E., Lundberg, J., 2001a. Stable isotope stratigraphy of a late Last Interglacial speleothem from Rana, northern Norway. Quaternary Research 56, 155–164.

Linge, H., Lauritzen, S.-E., Lundberg, J., Berstad, I.M., 2001b. Stable isotope stratigraphy of Holocene speleothems: examples from a cave system in Rana, northern Norway. Palaeogeography, Palaeoclimatology, Palaeoecology 167, 209–224.

McDermott, F., 2004. Palaeo-climate reconstruction from stable isotope variations in speleothems: a review. Quaternary Science Reviews 23, 901–918.

McGarry, S.F., Baker, A., 2000. Organic acid fluorescence: applications to speleothem palaeoenvironmental reconstruction. Quaternary Science Reviews 19, 1087–1101.

Mickler, P.J., Stern, L.A., Banner, J.L., 2006. Large kinetic isotope effects in modern speleothems. GSA Bulletin 118, 65–81.

O'Neil, J.R., Clayton, R.N., Mayeda, T.K., 1969. Oxygen isotope fractionation in divalent metal carbonates. The Journal of Chemical Physics 51, 5547–5558.

Perrette, Y., Delannoy, J.-J., Desmet, M., Lignier, V., Destombes, J.-L., 2005. Speleothem organic matter content imaging. The use of a Fluorescence Index to characterise the maximum emission wavelength. Chemical Geology 214, 193–208.

Proctor, C.J., Baker, A., Barnes, W.L., Gilmour, M.A., 2000. A thousand year speleothem proxy record of North Atlantic climate from Scotland. Climate Dynamics 16, 815–820.

Richards, D.A., Dorale, J.A., 2003. Uranium-series chronology and environmental applications of speleothems. Reviews in Mineralogy and Geochemistry 52, 407–460.

Rightmire, C.T., 1978. Seasonal variation in P_{CO2} and ^{13}C content of soil atmosphere. Water Resources Research 14, 691–692.

Schwarcz, H.P., 1980. Absolute age determinations of archaeological sites by uranium dating of travertines. Archaeometry 22, 3–24.

Schwarcz, H.P., 1989. Uranium series dating of Quaternary deposits. Quaternary International 1, 7–17.

Senesi, N., Miano, T.M., Provenzano, M.R., Brunetti, G., 1991. Characterisation, differentiation and classification of humic substances by fluorescence spectroscopy. Soil Science 152, 259–271.

Shopov, Y.Y., Ford, D.C., Schwarcz, H.P., 1994. Luminescent microbanding in speleothems: high-resolution chronology and paleoclimate. Geology 22, 407–410.

Smith, C.L., Fairchild, I.J., Spötl, C., Frisia, S., Borsato, A., Moreton, S.G., Wynn, P.M., 2009. Chronology building using objective identification of annual signals in trace element profiles of stalagmites. Quaternary Geochronology 4, 11–21.

Spötl, C., Fairchild, I.J., Tooth, A.F., 2005. Cave air control on dripwater geochemistry, Obir Caves (Austria): implications for speleothem deposition in dynamically ventilated caves. Geochimica et Cosmochimica Acta 69, 2451–2468.

Sundqvist, H.S., 2007. Speleothems as Environmental Recorders – a Study of Holocene Speleothems and their Growth Environments in Sweden. Unpublished Ph.D. thesis, Stockholm University, Stockholm, 57 pp.

Tan, M., Baker, A., Genty, D., Smith, C., Esper, J., Cai, B., 2006. Applications of stalagmite laminae to paleoclimate reconstructions: comparison with dendrochronology/climatology. Quaternary Science Reviews 25, 2103–2117.

van Beynen, P., Bourbonniere, R., Ford, D., Schwarcz, H., 2001. Causes of colour and fluorescence in speleothems. Chemical Geology 175, 319–341.

van Calsteren, P., Thomas, L., 2006. Uranium-series dating applications in natural environmental science. Earth-Science Reviews 75, 155–175.